Since January 2020 Elsevier has created a COVID-19 resource centre with free information in English and Mandarin on the novel coronavirus COVID-19. The COVID-19 resource centre is hosted on Elsevier Connect, the company's public news and information website.

Journal of Hazardous Materials 427 (2022) 128139

Contents lists available at ScienceDirect

Journal of Hazardous Materials

journal homepage: www.elsevier.com/locate/jhazmat

Unravelling multiple removal pathways of oseltamivir in wastewater by microalgae through experimentation and computation

Qasim M. Zeeshan [1], Shuang Qiu [1], Jia Gu, Abdul-Wahab Abbew, Zhengshuai Wu, Zhipeng Chen, Sai Xu, Shijian Ge [*]

Jiangsu Key Laboratory of Chemical Pollution Control and Resources Reuse, School of Environmental and Biological Engineering, Nanjing University of Science and Technology, Xiao Ling Wei 200, Nanjing 210094, Jiangsu, China

HIGHLIGHTS

- Biochemical endurance of *CS-N1* with ample AVD dissipation was first proposed.
- *CS-N1* growth and nutrient uptake robustness dropped for higher OT concentration.
- Elevated and validated EPS by 3D-EEM, FTIR and amide I revealed high bioadsorption.
- Bioadsorption and accumulation were the primary pathways for biodegradation (58.8%).
- DFT calculation elucidated algal enzyme-mediated biodegradation metabolites of OT.

GRAPHICAL ABSTRACT

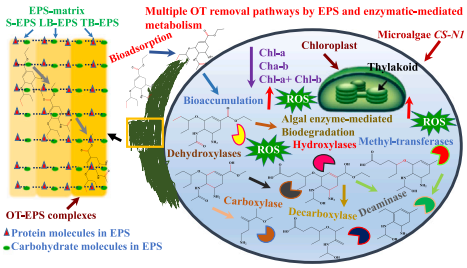

ARTICLE INFO

Editor: Dr. R. Debora

Keywords:
Antiviral drugs
Chlorella sorkiniana
Extracellular polymeric substances
Biodegradation
Quantum chemical calculation

ABSTRACT

Increased worldwide consumption of antiviral drugs (AVDs) amid COVID-19 has induced enormous burdens to the existing wastewater treatment systems. Microalgae-based bioremediation is a competitive alternative technology due to its simultaneous nutrient recovery and sustainable biomass production. However, knowledge about the fate, distribution, and interaction of AVDs with microalgae is yet to be determined. In this study, a concentration-determined influence of AVD oseltamivir (OT) was observed on the biochemical pathway of *Chlorella sorkiniana (C.S-N1)* in synthetic municipal wastewater. The results showed that high OT concentration inhibited biomass growth through increased oxidative stress and restrained photosynthesis. Nevertheless, complete OT removal was achieved at its optimized concentration of 10 mg/L by various biotic (82%) and abiotic processes (18.0%). The chemical alterations in three subtypes of extracellular polymeric substances (EPS) were primarily investigated by electrostatic (OT +8.22 mV vs. *C.S-N1* −18.31 mV) and hydrophobic interactions between EPS-OT complexes supported by secondary structure protein analysis. Besides, six biodegradation-catalyzed transformation products were identified by quadrupole-time-of-flight mass spectrometer and by density functional theory. Moreover, all the TPs exhibited log Kow $\leq$ 5 and bioconcentration factor values of $<$ 5000 L/kg, meeting the practical demands of environmental sustainability. This study broadens our understanding of microalgal bioadsorption and biodegradation, promoting microalgae bioremediation for nutrient recovery and AVDs removal.

* Corresponding author.
E-mail addresses: geshijian1221@njust.edu.cn, geshijian1221@126.com (S. Ge).
[1] Two authors contributed equally to this work.

https://doi.org/10.1016/j.jhazmat.2021.128139
Received 24 October 2021; Received in revised form 15 December 2021; Accepted 21 December 2021
Available online 24 December 2021

1. Introduction

The recent outbreak of the coronavirus (COVID-19) pandemic has profoundly increased the consumption of antiviral drugs (AVDs) worldwide (Kumar et al., 2020), leading to higher loads of AVDs in sewer lines and wastewater treatment plants (WWTPs). The transport of AVDs and their residues into the existing pharmaceutically-sick ecosystems further exacerbate the toxicological threats to human and environmental ecosystems (Rambabu et al., 2020). Previous studies demonstrated the inefficient removal of AVDs by conventional activated sludge processes mostly consisting of the physical and biological systems, which leaves AVDs and their metabolites in effluents (Funke et al., 2016; Mlunguza et al., 2020; Wang et al., 2021). The inclusion of tertiary treatments in WWTPs could further remove AVDs to certain extents but increase operational costs, limiting their use in practice (Qiu et al., 2021a). Therefore, the inadequate efficiencies of the current treatment approach critically encourage researchers to develop alternative technologies.

Microalgal bioremediation has attained increased attention in wastewater treatment systems, with competitive merits including nutrient recovery, greenhouse gas mitigation, and value-added biomass production (Ge et al., 2018; Qiu et al., 2021b). The application of microalgae in the removal of pharmaceutical and other inorganic contaminants like heavy metals has also been demonstrated as an ecological and sustainable reclamation approach (Chen et al., 2020b). For example, Matamoros et al. (2016) reported *Chlorella vulgaris* promoted 40% caffeine removal compared to the biological activated sludge process. Removal rates of sulfamethoxazole (99.3%) and methylpenantherine (99.8%) were achieved by *C. pyrenoidosa* and *Pseudokirchneriella subcapitata,* respectively (Xiong et al., 2020). Similarly, *Haematococcus pluvialis*, *C. vulgaris*, and *Selenestrum capricornutum* achieved almost complete removal of trimethoprim, azithromycin, and levofloxacin, respectively (Kiki et al., 2020). Nonetheless, due to increasing global consumption, knowledge of the occurrence, transport, and ecotoxicity implications of AVDs and their metabolites in downstream environments is essential. However, inadequate research has been conducted on AVD removals through sustainable approaches such as microalgae bioremediation. Taking into account the potentials of bioaccumulation and biomagnification of AVDs in food chains, microalgal cultivation in wastewater has the potential to simultaneously remove pharmaceutical pollutants and produce value-added biomass (Cheah et al., 2016; Rambabu et al., 2020). This study attempted to investigate the feasibility of microalgal systems as an alternative technology to minimize the AVD-triggered environmental pollution sustainably thereby filling a significant research gap.

To date, microalgae-mediated bioremediation of pharmaceutical contaminants has been believed to be governed by several biological pathways (Xie et al., 2020). However, some conflicting conclusions were reported on the specific microalgal removal pathways for pharmaceuticals. For example, Xiong et al. (2020) reported that biodegradation was the most effective way of degrading complex parent compounds, while Song et al. (2019) and Avila et al. (2021) insisted that bioaccumulation or bioadsorption was observed in eliminating florfenicol and carbamazepine, as well as chlorpyrifos (61.9%) and cypermethrin (60.1%), respectively. As such, it is essential to determine the most efficient elimination route, and minimal information is available on pollutant-algae interaction that exists after exposure to AVDs. Moreover, extracellular polymeric substances (EPS) have attracted focus as biofilm formers and exhibit potentials in adsorbing organic and inorganic pollutants, involving mechanisms such as chelation/complexation, electrostatic interactions, and is governed by different binding moieties (Jia et al., 2017). Previous reports have successfully delineated EPS functions in bioadsorption with attribution to the hydrophobicity of EPS proteins and also carbohydrates (Abbew et al., 2021; Hena et al., 2020). However, knowledge of the innermost mechanism of hydrophobicity and its manipulative nature resulting from pollutants interaction entails further research. Therefore, an in-depth analysis of the hydrophobic mechanisms of microalgal EPS is imperative, as it would aid in a better understating of the role of EPS in bioadsorption.

This study aimed to investigate microalgae (*Chlorella sorokiniana*)-based AVD removal with oseltamivir (OT) as the representative AVD due to its 80–90% distribution in sewage wastewaters through excretion (Nannou et al., 2020). Specifically, the physiological and growth dynamic responses of *C. sorokiniana* were investigated against different OT concentrations in synthetic municipal wastewater (SMW). Subsequently, the biological and abiological OT removal pathways were comprehensively evaluated, with a focus on bioadsorption via EPS analysis, and biodegradation by the quadrupole-time-of-flight mass spectrometer (UPLC-QToF-MS). Quantum chemical calculations were also conducted by the density functional theory (DFT) to confirm the biological metabolite structures of OT. The environmental toxicity profiles of OT metabolites were evaluated using the Estimation Programs Interface (EPI) Suite™ and Ecological Structure Activity Relationships (ECOSAR) class program. These findings offer new insights into the microalgal growth kinetics, nutrient and pharmaceutical removals from wastewater, enhancing the understanding of the microalgal-EPS hydrophobic mechanism, DFT-derived microalgal TPs of AVDs, and various ecotoxicity benchmarking of produced metabolites.

2. Materials and methods

2.1. Pre-culture of microalgae and oseltamivir

The microalgal species *C. sorokiniana* was isolated from municipal wastewater in Nanjing, China (accession NO.: MN906179), namely *C.S-N1*, and pre-cultured in BG-11 medium. Microalgal pellets were harvested by centrifugation at the exponential phase and transferred to SMW (Chen et al., 2020b). A stock solution of 1 mg/L OT (99% purity) was prepared in methanol. The detailed composition of BG-11 medium and SMW has been presented in Table S1-S2 in Supplementary information (SI) Section 1.

2.2. Experimental setup

The first experiment involved four OT treatment groups with different concentrations (i.e., 1-, 10-, 20-, and 30 mg/L) in SMW to assess microalgal physiological responses. Similar cultivation conditions were adopted as described in Section 2.1. All the groups were performed in triplicates with initial pHs at 7.0 ± 0.2. The parameters investigated included biomass growth, photosynthetic (the potential quantum efficiency photochemistry (Fv/Fm) and relative electron transport rate (rETR)) and oxidative cellular stress (reactive oxygen species (ROS)) indicators, nutrient uptake efficiencies (ammonium NH_4^+-N, phosphate PO_4^{3-}-P), and chlorophyll pigments analysis. The detailed information on pre-culture experimental conditions is presented in Section S1.

2.3. Microalgal biochemical analysis and three EPS-subtypes extraction

Microalgal growth was monitored daily by measuring the optical density at 680 nm (OD_{680}) using a spectrophotometer (UV-2100, U.S.). The intracellular ROS levels were determined for each treatment on Days 3, 5, and 8 using the ROS assay kit (Cat. S0033, Beyotime, Shanghai, China). Photosynthetic parameters, including Fv/Fm and rETR, were determined with a chlorophyll fluorometer measuring system (Water Pam, Walz GmbH, Effeltrich, Germany), as previously reported (Shen et al., 2020). The chlorophyll contents in cells were measured every other day using the spectrophotometer method, including the relative concentrations of chlorophyll a (Chl-a), chlorophyll b (Chl-b), total chlorophyll (Chl-a + Chl-b), and Chl ratio (Chl-a/Chl-b). The details for the above-mentioned tests are shown in SI Section S2.

At the end of the experiment, three microalgal EPS-subtypes,

including soluble-EPS (S-EPS), loosely-bound EPS (LB-EPS), and tightly-bound EPS (TB-EPS), were extracted by the modified heating method (Wang et al., 2020b). The characterization of the extracted EPS solution was conducted by the Fourier transform infrared spectroscopy (FTIR, NICOLETIS 10, Thermo Scientific Instruments LLC, U.S.). Moreover, three-dimensional-excitation emission matrix (3D-EEM) analysis was performed with a fluorescence spectrometer (F-7000, Hitachi, Japan). The role of secondary structure hydrophobic proteins of EPS in adsorption was analyzed on the second-derivatized and deconvoluted spectra of the amide I region (1600–1700 cm^{-1}) through the quantitative determination of each peak area using Peakfit software (version 4.12, Seasolve Software Inc.). The details of EPS-subtype extraction and characterization are presented in Section S3.

2.4. Evaluation of different removal pathways with their relative contribution

Based on the above experimental results, the second experiment was conducted to evaluate different removal pathways of OT by *C.S-N1*, by selecting the 10 mg/L OT group and the control. Similar cultivation was carried out as the first experiment. In general, pharmaceutical elimination routes were separated into two parts: biotic removal pathways (i.e., bioadsorption, bioaccumulation, biodegradation) and abiotic removal pathways (i.e., hydrolysis, photolysis) (Xiong et al., 2017). Details of possible removal pathways with respective contributions are summarized in Section S4 and Table S3.

2.5. Quantification and computation of OT metabolites involved in biodegradation

The dissolved, bioadsorbed, bioaccumulated, and biodegraded fractions of OT were determined by a recent method (Kiki et al., 2020). Firstly, the residual OT concentration was routinely quantified using HPLC (instrument: U3000-UV, Agilent, USA) at electrospray ionization (+ESI) mode. Biodegradation-based TPs were identified using UPLC-QToF-MS/MS in high resolution-mass spectrometry (HRMS) with positive ESI mode. To explore the environmental implications of the produced TPs, their persistence (P), bioaccumulation (B), and ecotoxicity (T) were assayed by EPI Suite™ software (version 4.11) and ECOSAR class program developed by United States Environmental Protection Agency (US-EPA) (Xie et al., 2020). The description of removal mechanisms for OT, HPLC operating conditions, TPs identification by UPLC-QToF-MS, and PBT parameters are provided in Section S4 and Fig. S2.

DFT was applied for the structural calculations of OT metabolites in the Gaussian 16 package (Frisch et al., 2019). The B3LYP functional protocol assessed the geometrical optimizations, and the 6–311 + + G (3df, 3pd) basis set was employed for observing all the atoms (Liu et al., 2019). The solvation model density (SMD) was applied for the solvation effect to explore the reaction energy pathway for all the reactants and products (Luo et al., 2020). Besides, the vibrational frequency calculation was provided to crosscheck the stable point on the potential energy surface. Finally, all the reported energies in the study were obtained with zero-point energy correction and given in Kcal/mol at 298.15 K and 1 atm.

2.6. Statistical analysis

One-way analysis of variance (ANOVA) with a post-hoc Tukey's test or t-test was conducted at a significant level of 0.05 with Graphpad Prism (Version 8.4.3, GraphPad Software Inc., USA). The presented results are the average values ± standard deviation from the independently replicated experiments (n = 3).

3. Results and discussion

3.1. OT impacted the biochemical viability of C.S-N1

3.1.1. OT induced biomass reduction, nutrient uptake suppression, and oxidative stress elevation

Compared to the control, the exposure to OT concentrations (1, 10, 20, and 30 mg/L) resulted in descending trends in the growth kinetics of *C.S-N1* in SMW. As presented in Fig. 1**a**, a dose-dependent biomass growth inhibition was observed in *C.S-N1* . Specifically, a significantly reduced growth was observed in both the 20 mg/L and 30 mg/L OT groups (0.27 g/L and 0.24 g/L, respectively) compared to the control and lower OT treated groups ($p < 0.01$ one-way ANOVA with Tukey's post-hoc test). This observation was consistent with previous reports showing similar suppressions on microalgal growth under high pharmaceutical levels (Gomaa et al., 2021; Rempel et al., 2021). However, the biomass was increased in all OT treatment groups in the exponential growth periods on later days (Days 2–5) ($p < 0.05$, one-way ANOVA with Tukey's post-hoc test), implying the gradual acclimatization of *C.S-N1* under relatively stable pH conditions of 7.0–9.0 (Fig. 1a, Fig. S3) (Zhang et al., 2021b). The results were in line with previous literature which suggested that the pH range of 6–10 was optimal for microalgae cultivation (Chia et al., 2018). This further elucidated that the growth inhibition was non-pHdependent and proportional to the increasing OT doses. Table 1 compares the growth performance of *C.S-N1* until Day 10 under different OT concentrations. As indicated by the similar specific growth rates, no differences were observed in the growth performance among the control and the first two lower OT groups ($p > 0.05$, one-way ANOVA with Tukey's post-hoc test). However, the respective 3.0-fold and 4.0-fold reduction in biomass productivity were observed in the 20 mg/L and 30 mg/L OT groups in comparison to the control ($p < 0.001$, one-way ANOVA with Tukey's post-hoc test). As expected, the highest doubling time (46.82 ± 0.2 h) and the lowest.

biomass growth rate (0.35 ± 0.1/d) were achieved in the 30 mg/L OT group. These results indicated a concentration-oriented adaptive response of *C.S-N1* to OT levels lower than 20 mg/L.

The different growth performances correlated well with the cellular ROS levels in the five treatment groups. As shown in Fig. 1b, the cellular ROS generation significantly increased with the increasing OT concentrations on the three tested days ($p < 0.05$, one-way ANOVA with Tukey's post-hoc test). For example, a 69% higher ROS was observed in the 30 mg/L group compared to the control on Day 3 ($p < 0.001$, one-way ANOVA with Tukey's post-hoc test). This was in line with a recent study that showed an instant rise in ROS levels in *C. pyrenoidosa* with exposure to butyl xanthate and nickel mixture between 1–20 mg/L concentration (Li et al., 2021). It was reported that the presence of pollutants such as nanoplastics induced mitochondrial hyperpolarization in microalgae, further accelerating the ROS levels to resist the toxic effects (Wang et al., 2020a). Nonetheless, the ROS levels in higher OT groups tended to decrease during later days. A 50.0% decrease of ROS was observed on Day 8 compared with Day 3 (62.9 ± 2.00 vs. 121.6 ± 4.10, respectively), further supporting the gradual acclimation of *C.S-N1* to OT-induced stress (Fig. 1b). Additionally, *C.S-N1* sufficiently neutralized the ROS levels in the four lower OT groups with no significant differences on Day 8 (Fig. 1b). This observation could be consistent with the previous findings that an acceptable dose of a stressful stimulus could trigger an adaptive response against the stress factor (Peter et al., 2021).

Delayed nutrient uptake performance (i.e., uptake kinetics, uptake efficiencies, uptake rate) was observed for NH_4^+-N and PO_4^{3-}-P with the supplementation of different OT treatment groups (Fig. 1c-d). Specifically, NH_4^+-N was completely assimilated in the control on Day 3 with a 28.1 ± 0.3% higher uptake rate compared to the 30 mg/L OT group ($p < 0.05$, one-way ANOVA with Tukey's post-hoc test). Similarly, a 54.3 ± 0.3% PO_4^{3-}-P removal in the control while only a 38.0 ± 0.6% removal for the 30 mg/L OT group was achieved on Day 10 ($p < 0.05$,

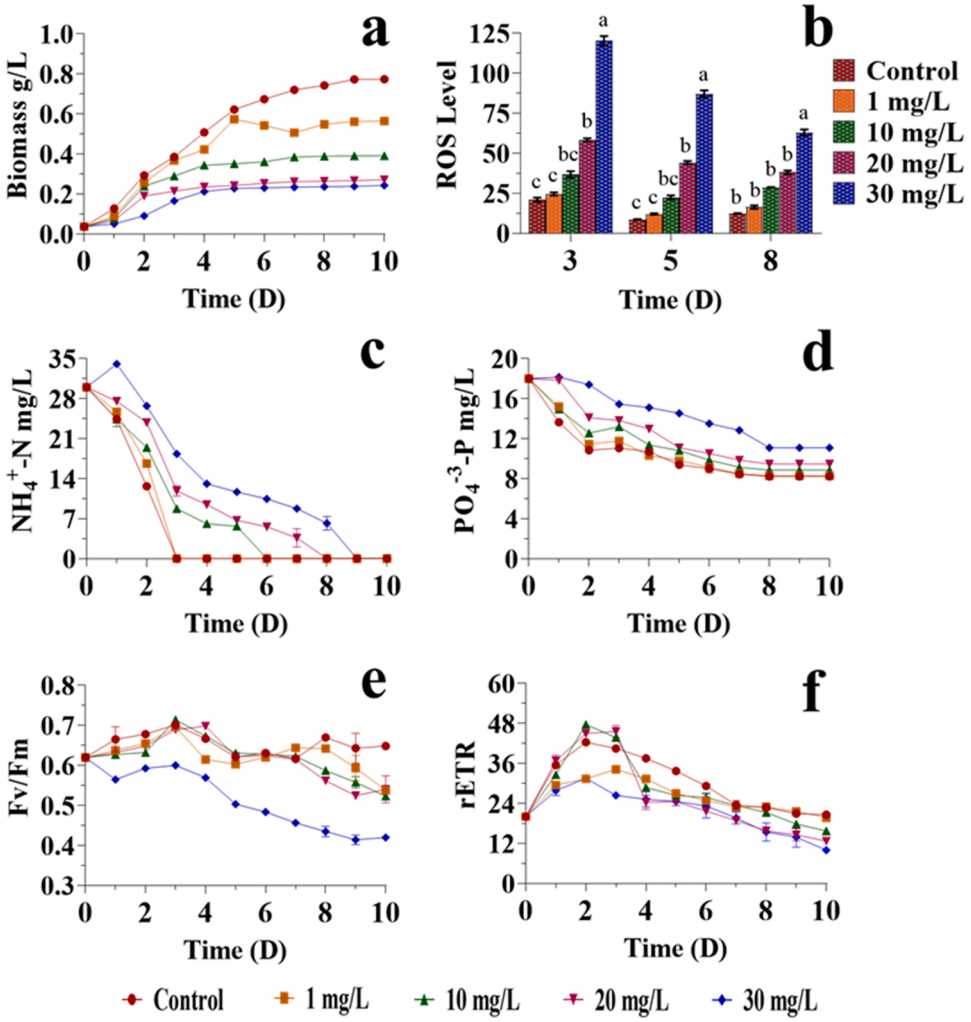

Fig. 1. Influence of various OT treatment groups on (a) the biomass content (g/L) (b) ROS (c) NH_4^+-N (d) PO_4^{3-}-P removal efficiency (e) potential maximum quantum efficiency photochemistry (Fv/Fm) and (f) relative electron transport rate theory (rETR) of *C.S-N1*.

Table 1
Growth performance of C.S-N1 under different OT concentrations.

OT treatment group	Specific growth rate (μ/d)	Biomass productivity (g/ (L•d))	Doubling time (h)	NH_4^+-N removal (mg/ (L•d))	PO_4^{3-}-P removal (mg/L•d)
Control	0.49 ± 0.2^{a}	0.11 ± 0.02^{a}	33.62 ± 0.6^{d}	10.53 ± 0.03^{a}	1.22 ± 0.01^{a}
1 mg/L	0.45 ± 0.2^{a}	0.09 ± 0.04^{a}	36.43 ± 0.2^{cd}	10.14 ± 0.4^{a}	1.21 ± 0.03^{a}
10 mg/L	0.42 ± 0.3^{a}	0.07 ± 0.03^{ab}	39.19 ± 0.2^{c}	5.67 ± 0.02^{b}	1.14 ± 0.02^{b}
20 mg/L	0.37 ± 0.2^{b}	0.04 ± 0.03^{bc}	44.34 ± 0.2^{b}	3.75 ± 0.03^{cd}	1.06 ± 0.5^{bc}
30 mg/L	0.35 ± 0.1^{b}	0.03 ± 0.01^{c}	46.82 ± 0.2^{a}	2.97 ± 0.05^{d}	0.74 ± 0.1^{c}

one-way ANOVA with Tukey's post-hoc test). This observation was also supported by the nutrient removal rate, as indicated by the 4.0-fold (2.97 ± 0.05 mg/(L•Day)) and 1.0-fold (0.74 ± 0.1 mg/(L•Day)) reductions for the 30 mg/L OT group compared to the control, respectively. BothN and P are the core components of nucleic acids and proteins. P plays a role in energy conservation through adenosine triphosphate, polyphosphate and information delivery through post-translational modification of proteins (Hu et al., 2020). Therefore, the deficit assimilation of N and P in higher OT levels might contribute to the hampered microalgal growth and physiological disruption (Hu et al., 2020). However, *C.S-N1* adapted to higher OT dose-driven harsh environments during progressive cultivation days with sufficient assimilation of NH_4^+-N and PO_4^{3-}-P and improved growth, which might be attributed to the activation of the algal antioxidant system. A similar observation was also reported, demonstrating that NH_4^+-N and PO_4^{3-}-P might have a supportive role in pollutant toxicity alleviation in microalgae (Chawla et al., 2020). Thus, the progressive assimilation of nutrients might also favor *C.S-N1* in withstanding the potential cellular damage. Overall, the uptake of both NH_4^+-N and PO_4^{3-}-P optimized the response against OT-induced stress conditions on later days with feasible growth recovery and biomass production.

3.1.2. OT inhibited photosynthetic activities of C.S-N1

Reduced biomass production was associated with decreased photosynthetic efficiency and reduced pigment synthesis, possibly due to the diminished absorption of light energy through electron transfer blockade (Mao et al., 2021). Two important indicators of algal photosynthetic status (i.e., Fv/Fm and rETR) were assessed in *C.S-N1* during the 10-day incubation. Particularly, the initial Fv/Fm value (0.62) was higher than 0.5 (Fig. 1e), suggesting satisfactory physiological

endurance in all groups towards ambient cultivation conditions (light, temperature, light: dark cycle) (Abbew et al., 2021). On Day 3, however, the Fv/Fm increased in all treated groups and subsequently declined. Compared to the control, the 30 mg/L OT group exhibited the most significant decrease in the Fv/Fm values (36.1 ± 0.02%) on Day 10. Significant reductions (17.2 ± 0.8%, 19.01 ± 0.4%, and 15.6 ± 0.3%) were observed in 1 mg/L, 10 mg/L and 20 mg/L treatments ($p < 0.05$, one-way ANOVA with Tukey's post-hoc test). The decline in the Fv/Fm values indicated photosynthetically unhealthy cells, inferring OT-induced susceptibility to photoinhibition in *C.S-N1*.

Consistent with the Fv/Fm results, a transient increase in rETR values was observed in all groups till Day 3, followed by a decline in all groups on subsequent days (Fig. 1f). Diminished rETR values in the >10 mg/L groups corresponded to the inhibited electron transport rates, indicating reduced carbon-assimilation capacity. This hinted that the OT treatment has considerable dose- and time-oriented effects on photosynthetic efficiencies, with the following considerations. Firstly, the exposure to higher OT concentrations might adversely impact the Fv/Fm due to the reduced light absorption, restricting the electron flow rate from H_2O to NADP by PSII electron carriers (Zhang et al., 2020). Secondly, this could also trigger the retardation of PSII in *C.S-N1* through secondary effects on several metabolic pathways, mainly by producing superoxide radicals and elevating non-photochemical quenching of excitation energy (Qiu et al., 2021). Moreover, these high-energy radicals strongly disrupted chloroplast proteins and membranes of photosynthetic cells, hence reducing the overall photosynthetic efficiency in *C.S-N1* (Shen et al., 2020). Additionally, a recent study depicted that the primary site of photosynthetic damage is the light reaction centers (Mao et al., 2021). This implies that OT-prompted decline in photosynthesis defines a reduction in light energy conversion to chemical energy, thereby decreasing microalgal growth.

3.1.3. OT reduced chlorophyll contents in C.S-N1

Chlorophyll contents (Chl-a and Chl-b) are one of the integral components that indicate microalgal photosynthetic robustness in response to the external environments. As shown in Fig. 2a, Chl-a values were significantly decreased in both 20 mg/L and 30 mg/L OT groups ($p < 0.05$, one-way ANOVA with Tukey's post-hoc test), while no remarkable variations of Chl-b were observed between the control and the 1 mg/L group (Fig. 2b). Moreover, a small and significant difference was observed in the control versus the 10 mg/L OT group on Day 10 ($p < 0.05$, one-way ANOVA with Tukey's post-hoc test). This indicated that *C.S-N1* might have potential tolerance against the lower OT concentration, which was further supported by the visual comparison on each day with nearly similar culture color at lower OT groups (Fig. S4).

Compared with the control, the recorded inhibition percentages of Chl-a on Day 10 in the 30 mg/L, 20 mg/L, 10 mg/L and 1 mg/L OT groups were 53.1 ± 0.4%, 47.1 ± 0.6%, 29.7 ± 0.1%, and 24.8 ± 0.03%, respectively ($p < 0.05$, one-way ANOVA with Tukey's post-hoc test). Chl-b, on the other hand, is deemed alternatively a radical accessory pigment that is often converted into Chl-a under stressed environments (Chu et al., 2021). Hence, a lower Chl-b level was recorded on Day 10 in all OT groups compared to the control, implying an altered photosynthetic metabolism in response to high OT-induced oxidative stress (Fig. 2b). Additionally, the total Chl concentration showed a similar trend as Chl-a and Chl-b (Fig. 2c). Moreover, an obvious negative correlation between the OT level and the ratio of Chl-a to Chl-b was observed and the maximum value of 2.7 ± 0.02 was achieved in the 30 mg/L OT group on Day 10 ($p < 0.01$, one-way ANOVA with Tukey's post-hoc test) (Fig. 2d). OT-incited imbalances in the optimal Chl-a/Chl-b ratio impacted the microalgal light energy harvesting efficiency, resulting indecreased photosynthesis. Particularly, the lower chlorophyll contents observed in the 20 mg/L and 30 mg/L OT groups were primarily due to the OT-induced inhibition of NADH dehydrogenase subunits in the electron transport chain. This resulted in higher oxidative stress response, peroxidation of chloroplast membranes, and reduced chlorophyll density (Carstensen et al., 2018; Gao et al., 2017). A recent study indicated that exposure to polystyrene nanoplastics

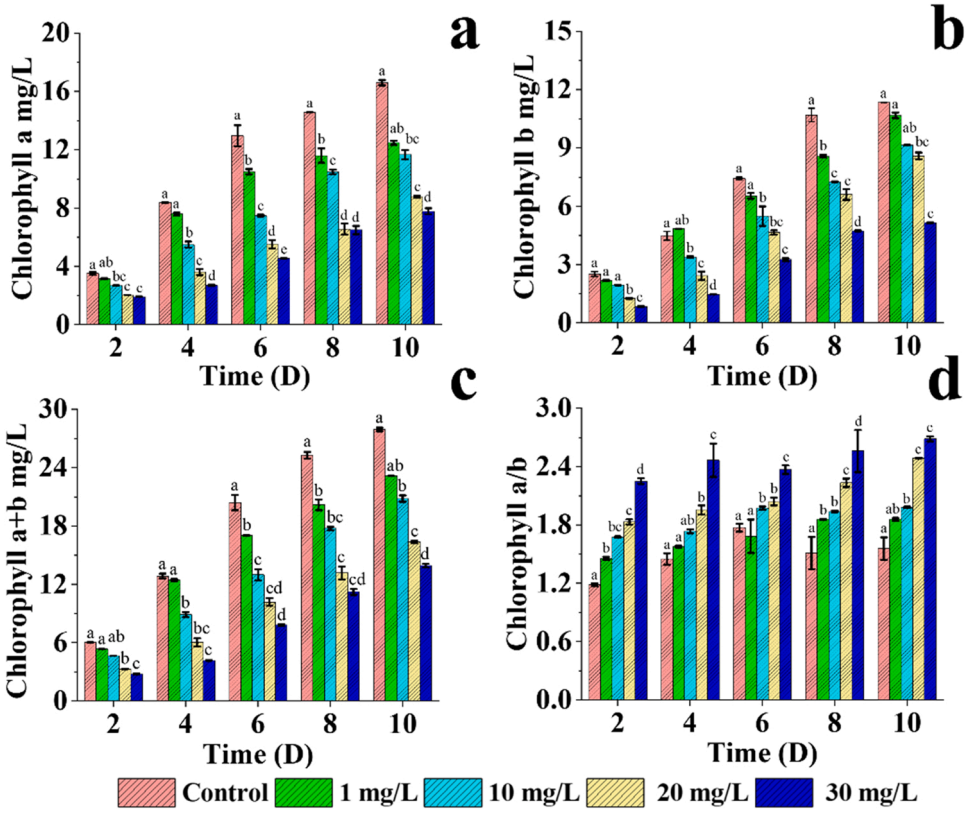

Fig. 2. The effect of OT on chlorophyll profiles of *C.S-N1* (a) Chlorophyll-a (b) Chlorophyll-b, (c) Chlorophyll-(a+b), (d) Chlorophyll-a/b over 10 Days of cultivation.

ruptured chloroplast membranes and deteriorated chloroplast viability of *Platymonas helgolandica* (Wang et al., 2020a). Another possible explanation for the reduced chlorophyll level was that higher OT concentrations would disturb PSII metabolic pathway and invoke the non-photochemical quenching of excitation energy, producing radicals like singlet and triplet chlorophyll energized states (Zhang et al., 2021a). Consequently, these highly reactive molecules could trigger oxidative damage to the chloroplast physiology, reducing the chlorophyll synthesis at high OT treatment groups.

3.2. Concentration-dependent removal pathways of OT by C.S-N1

The removal dynamics of OT by *C.S-N1* were evaluated through five elimination pathways, including abiotic losses (hydrolysis and photolysis) and biotic losses (bioadsorption, bioaccumulation, and biodegradation). As revealed in Fig. 3a, OT was completely removed in two lower OT groups (1 mg/L and 10 mg/L), while only 54.0–63.0% removal was observed in the 20 mg/L and 30 mg/L groups, respectively. Therefore, the 10 mg/L OT treatment group was selected to investigate the mechanism-specific OT removal kinetics. As shown in Fig. 3b, the primary OT removal was driven by the biotic losses (82.0%) in comparison with the abiotic losses (18.0%). A detailed description of the respective removal mechanisms is provided in the following sections.

3.2.1. Hydrolytic and photolytic removal pathways

The abiotic control experiments under illuminated or dark conditions yielded the photolytic and hydrolytic removals of OT. As shown in Fig. 3b, the contribution of hydrolysis to the total OT removal was 8.0% which was similar to a recent study demonstrating an approximately 3% hydrolysis of ciprofloxacin by *Chlamydomonas* sp. (Xie et al., 2020). This low OT removal by hydrolysis was likely due to its relatively higher water partitioning coefficient and lower water solubility with the log Kow of 0.95 (Olisah et al., 2021). Moreover, photolysis induced 9.0% OT removal, and it was in agreement with a 5–14% photolytic removal of sulfamerazine, sulfamethoxazole, levofloxacin, and flumequine by microalgae (Kiki et al., 2020). The photolytic loss was primarily governed by light irradiation through the cleavage of C-H and C-N bonds, hydrogen abstraction of radicals, disproportionation of alkyl radicals, and the consecutive free-radical oxidations (Luo et al., 2020). In this study, it was believed that photo-transformation of OT was possibly triggered by the hydroxyl radical ($OH^{\cdot}$) formation during the photolysis of nitrate present in the culture medium (Gen et al., 2019; Zhang et al., 2018). Hence, the rapid consumption of nitrate by *C.S-N1* led to the lower photolytic removal of OT compared with the other biotic processes (Fig. 3b).

3.2.2. Bioadsorption induced by electrostatic and hydrophobic interaction

Various studies have debated on microalgal bioadsorption potentials under higher concentrations of pollutants (Ubando et al., 2021; Wang et al., 2020c). However, the underlying mechanism remains unknown. Bioadsorption, corresponding to electrostatic charge difference and hydrophobicity mechanisms, is often governed by EPS adsorption (Wang et al., 2020b). Consistently, the average zeta potential of *C.S-N1* was −18.31 mV compared to the positive zeta potential (+8.22 mV) of OT in this study (Fig. S5). Therefore, the definite electrostatic charge neutralization between *C.S-N1* and OT molecules was one of the integral factors contributing to bioadsorption.

Microalgal EPS was systematically analyzed to gain better insights into EPS-mediated hydrophobic interactions with subsequent OT bioadsorption. For this, the 30 mg/L OT group with the most stressful condition was selected and compared with the control to investigate bioadsorption and chemical alterations in three EPS-subtypes (i.e., S-EPS, LB-EPS, TB-EPS) as follows.

(1) Qualitative analysis with 3D-EEM and FTIR spectroscopy. The 3D-EEM results (Fig. S6) demonstrated that fluorescence intensities of EPS-subtypes increased with increasing OT concentration, with more concentrated peaks in the 30 mg/L group, versus lower peak intensities in the control. The concentrated peaks revealed increased secretions for hydrophobic proteins in all EPS-subtypes for the 30 mg/L OT group, implying that more binding sites were available to form OT-EPS complexes. Specifically, the Ex/Em peaks at 230–250/330–350 nm, 270–330/300–375 nm, and 300–345/400–420 nm corresponded to tyrosine-, tryptophan-like proteins, and humic acid compounds, respectively (Wang et al., 2020b). However, humic acid-related peaks were only detected in S-EPS samples of both groups (Hena et al., 2020).

As shown in Fig. 4a-b, six predominant FTIR spectral bands ranging from 1044 to 3365 cm^{-1} were observed in both samples. Particularly, the bands between 3297 and 3365 cm^{-1}, 2888–2945 cm^{-1}, and 1653 cm^{-1}, corresponded to O-H bonded with N-H stretching vibrations, C-H stretching vibrations, and C═O stretching vibrations in both carbohydrates and proteins (Jia et al., 2017; Wang et al., 2020b). Besides, the peaks at 1457–1507 cm^{-1}, 1108–1128 cm^{-1}, and 1044–1054 cm^{-1} were assigned to N-H deformation vibrations, C-O-C, and C-H ring vibrations, respectively (Chen et al., 2021; Wang et al., 2020b). The presence of characteristic functional groups in EPS-subtypes further suggested the involvement of hydrophobic protein and carbohydrate molecules, contributing to OT adsorption. Nevertheless, all these spectra comparably differed in their transmittance (%), and S-EPS was prominent relative to LB-EPS and TB-EPS in both samples. The C═O group was ascribed to the carboxylic group of proteins, indicating the acidic nature of algal EPS. This comprises a negative charge, which may further facilitate bioadsorption. Importantly, EPS structures expand and become loose after binding, facilitating the improved mass transfer and pollutant capture. Similarly, a previous study reported spontaneously accelerated binding processes of sulfamethazine with EPS through hydrophobic interactions (Zou et al., 2021). These EPS protein and carbohydrate molecules are vigorously

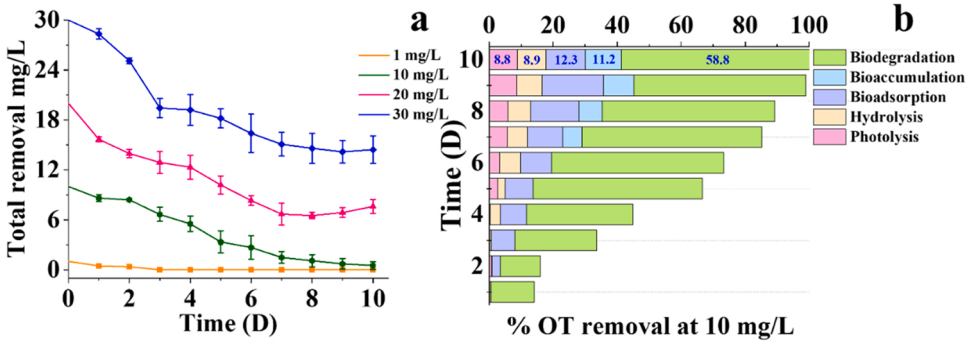

Fig. 3. Time course (Days) profiles of (a) 1 mg/L, 10 mg/L, 20 mg/L, and 30 mg/L of OT dissipation (b) percentage removal kinetics of OT by biodegradation, bioaccumulation, bioadsorption, hydrolysis, and photolysis at 10 mg/L.

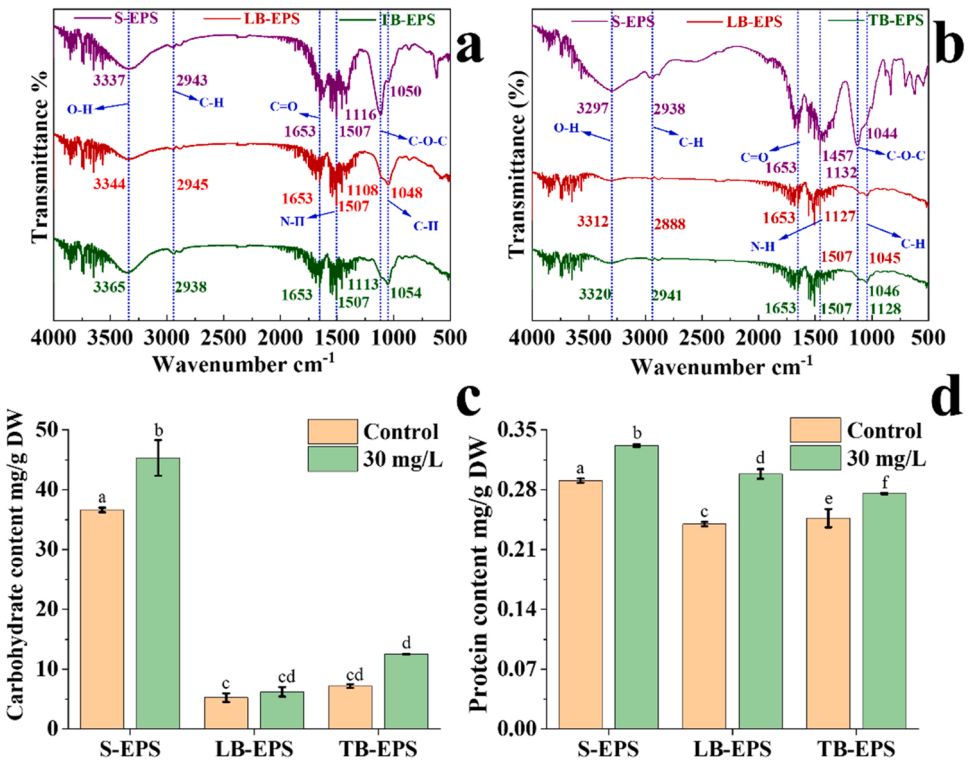

Fig. 4. Chemical composition of three EPS-subtypes. Fourier transform infrared (FTIR) spectroscopy (4000–500 cm^{-1}) of S-EPS, LB-EPS, and TB-EPS in (a) the control, (b) 30 mg/L OT group. Carbohydrate and protein profiles of S-EPS, LB-EPS, and TB-EPS in samples for (c) the control, (d) 30 mg/L OT group.

hydrophobic, hence facilitating bioadsorption (Naveed et al., 2020). Asharuddin et al. (2021) reported that the side chains of carbohydrates (e.g., glucose, rhamnose, and galactose) served as viable binding sites due to the long-carbon backbone and actively promoted EPS interactions. This was also supported by previous studies, which suggested that the C-H groups in carbohydrates interacted with π-electron of heterocyclic aromatic compounds forming C-H-π bonds through van der Waals interaction (Escobar and Ballester, 2021; Hena et al., 2020). Considering these observations, it can be concluded that OT stimulated the EPS protein and carbohydrate secretions. This made more functional groups available especially in the 30 mg/L group and demonstrated interactions with OT molecules. Therefore, the increasing EPS secretions would offer more binding sites with OT, facilitating the complexation and adsorption as well as the subsequent degradation.

(2) Quantitative analysis with EPS-subtypes and secondary structure proteins. It was found that higher protein and carbohydrate levels were achieved in the 30 mg/L OT group in all EPS-subtypes, indicating elevated EPS secretions (Fig. 4c-d). The highest carbohydrate (45.32 ± 0.03 mg/g DW) and protein (0.33 ± 0.001 mg/g DW) contents were reported in the S-EPS of 30 mg/L group versus relatively lower carbohydrate (36.6 ± 0.02 mg/g DW) and protein (0.29 ± 0.03 mg/g DW) contents in those of the control ($p < 0.005$, t-test). It was believed that these competitively elevated EPS contents offered protective strategies for microalgal survival and growth in OT-stressed environments. Moreover, a recent study suggested that EPS production is a metabolism-independent process, hence, increased EPS secretions were reported despite compromised growth and inhibited photosynthetic efficiencies, and therefore, our results were strongly coherent with these previous findings (Mohite et al., 2017).

Alternatively, FTIR spectra in the1600–1700 cm^{-1} region were also analyzed by the second derivative resolution curve fitting and deconvolution process to explain the differences in the protein secondary structures of the amide I region and the hydrophobic mechanism (Lu et al., 2021). As shown in Fig. 5, considerable differences were observed in second derivative peaks between the control (Fig. 5a-c-e) and the 30 mg/L group (Fig. 5b-d-f). This was ascribed to the OT-triggered structural rearrangement and conformational changes in the EPS proteins.

Table 2 illustrates the relative proportions of the secondary structure proteins in both groups. Specifically, the proportions of *β*-sheet, which exhibits sorptive and surface-active action and confers enhanced bonding strength and stiffness, considerably increased in all EPS-subtypes in the 30 mg/L group. The OT-induced elevated *β*-sheet level resulted in improved complexation, physical adsorption, as well as precipitation (Wu et al., 2019). Although no remarkable differences were found in random coil and *β*-turn, the proportions of *α*-helix significantly decreased, further indicating the distinctive involvement in the adsorption (Farhadian et al., 2021). Additionally, the hydrophily degree of the EPS-subtypes in the 30 mg/L group exhibited 28.6%, 31.9%, and 22.2% less hydrophily in comparison with the control. Therefore, the OT-influenced higher EPS hydrophobicity promoted the formation of the OT-EPS aggregates, and the accelerated carbohydrate and protein secretions facilitated the bioadsorption (Chen et al., 2021).

It should be noted that a similar removal contribution (11.3%) was obtained for the bioaccumulation process as that of bioadsorption, both of which are involved as initial steps during the microalgal OT removal processes. Specifically, after entering the microalgal cells, the bioadsorbed OT molecules were converted to bioaccumulated fractions, which subsequently stimulated the detoxification mechanisms. This further promoted biodegradation catalyzed by the cytochrome-P450 enzyme system (Wang et al., 2018; Xiong et al., 2018).

3.3. Biodegradation: metabolites identification and computation confirmation

The specific biodegradation process was systematically investigated through both the identification of metabolites and the DFT computation. The UPLC-QToF-MS analysis indicated that a total of 6 transformation

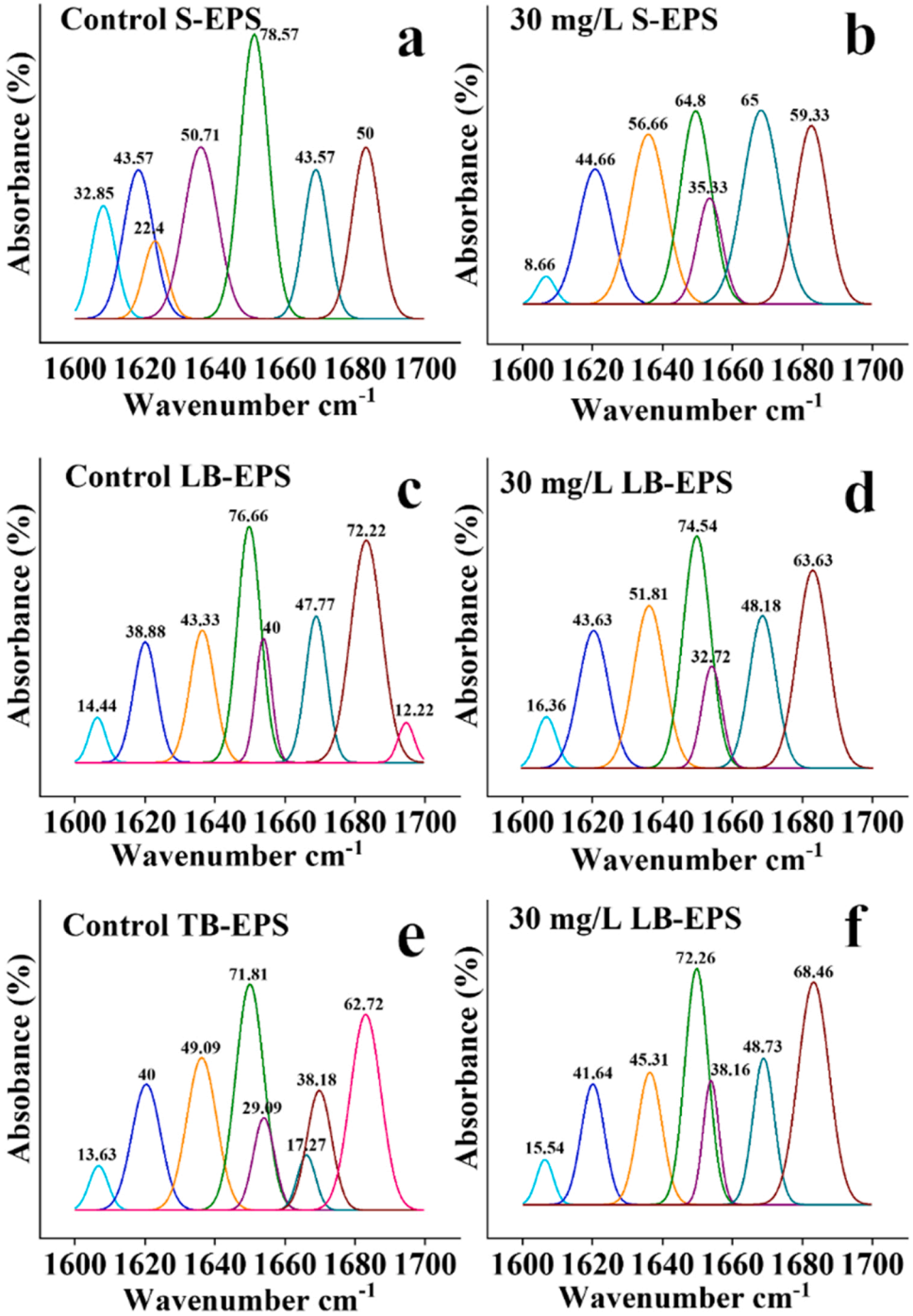

Fig. 5. Second derivative resolution curve-fitted amide I region (1600–1700 cm^{-1}) of (b) S-EPS, (c) LB-EPS, and (d) TB-EPS in control and in the (f) S-EPS, (g) LB-EPS, and (h) TB-EPS of the 30 mg/L group.

products (TP-360, TP-301, TP-299, TP-245, TP-197, and TP-128) were detected to be involved in the biodegradation process. No photolytic TPs were observed due to the lower removal proportion (8.8%, Fig. 3b) in this study with reference to literature (Chen et al., 2020a; Omar et al., 2017).

Fig. 6 illustrates the proposed biodegradation reactions with specific metabolites, considering the Gibbs free energy ΔG (Kcal/mol) scheme, chemical formula, and structural description for all TPs and related reactions (Table S4).

Specifically, the negative ΔG values in all the reactions indicated the spontaneous nature of transformations. The formation of TP-360 from OT (*m/z* 312) was maximally exothermic and most energetically favorable (ΔG −856.16 Kcal/mol). This conversion was attributed to successive hydroxylation and carboxylation of OT (*m/z* 312) at the carbon (C)11 site (Fig. 6b). The highest absolute value of ΔG for this reaction suggested that the C11 site was more active than other C sites (Luo et al., 2020), which might be related to the action of hydroxylases and carboxylases during algal metabolism (Ding et al., 2017; Xiong et al., 2018). Alternatively, the parent compound (*m/z* 312) might directly undergo demethylation and hydroxylation at the C11 site and transform into TP-301 (ΔG −13.42 Kcal/mol). This is evidenced by a study demonstrating that algal hydroxylases and demethylases from the cytochrome P450 family were actively involved in xenobiotics metabolism (Ding et al., 2017; Xiong et al., 2018). Progressively, the C3 site

Table 2
The relative proportion of secondary protein structures in control versus 30 mg/L OT group. Bands at 1610–1640 cm^{-1} and 1680–1695 cm^{-1} were attributed to β-sheet, and bands at 1640–1650 cm^{-1}, 1650–1660 cm^{-1}, and 1660–1680 cm^{-1} corresponded to strong absorption by random coil, α-helix, and β-turn, respectively. Hydrophily was calculated by dividing α-helix to the β-sheet+random coil.

Category	β-sheet (%)	α-helix (%)	random coil (%)	β-turn (%)	Hydrophily
Control					
S-EPS	43.29	26.5	19.51	10.70	0.42
LB-EPS	47.17	29. 34	14.03	9. 46	0.47
TB-EPS	38.36	27.47	21.55	12.62	0.45
30 mg/L OT					
S-EPS	53.72	21.45	17.47	7.36	0.30
LB-EPS	51.69	20.71	14.47	13.13	0.32
TB-EPS	52.93	22.56	9.93	14.58	0.35

in TP-360 could be attacked by C-C bond cleavage, and simultaneous dehydroxylation produced TP-299. This reaction was linked with a highly negative ΔG of − 448.59 (Kcal/mol), demonstrating that it could quickly proceed and get catalyzed by algal dehydroxylases (Avila et al., 2021). However, TP-299 was not detected in the later cultivation days, possibly due to its rapid metabolism into other TPs. Guengerich (2018) reported that cytochrome P450 enzymatic reactions involve multiple steps where the product of one reaction is a substrate of the subsequent reaction with the same or different enzymes. In this study, it was believed that six TPs were produced through progressive breakdown into simpler products. For example, the removal of ethoxypropanol from TP-360 coupled with deamination yielded TP-245, provided that deamination could be triggered by algal deaminases (Hu et al., 2021). The negative value of ΔG (−20.30 Kcal/mol) further supported that this reaction was kinetically feasible and could proceed at ambient conditions (Liu et al., 2019). Similarly, TP-197 was generated by cyclohexane

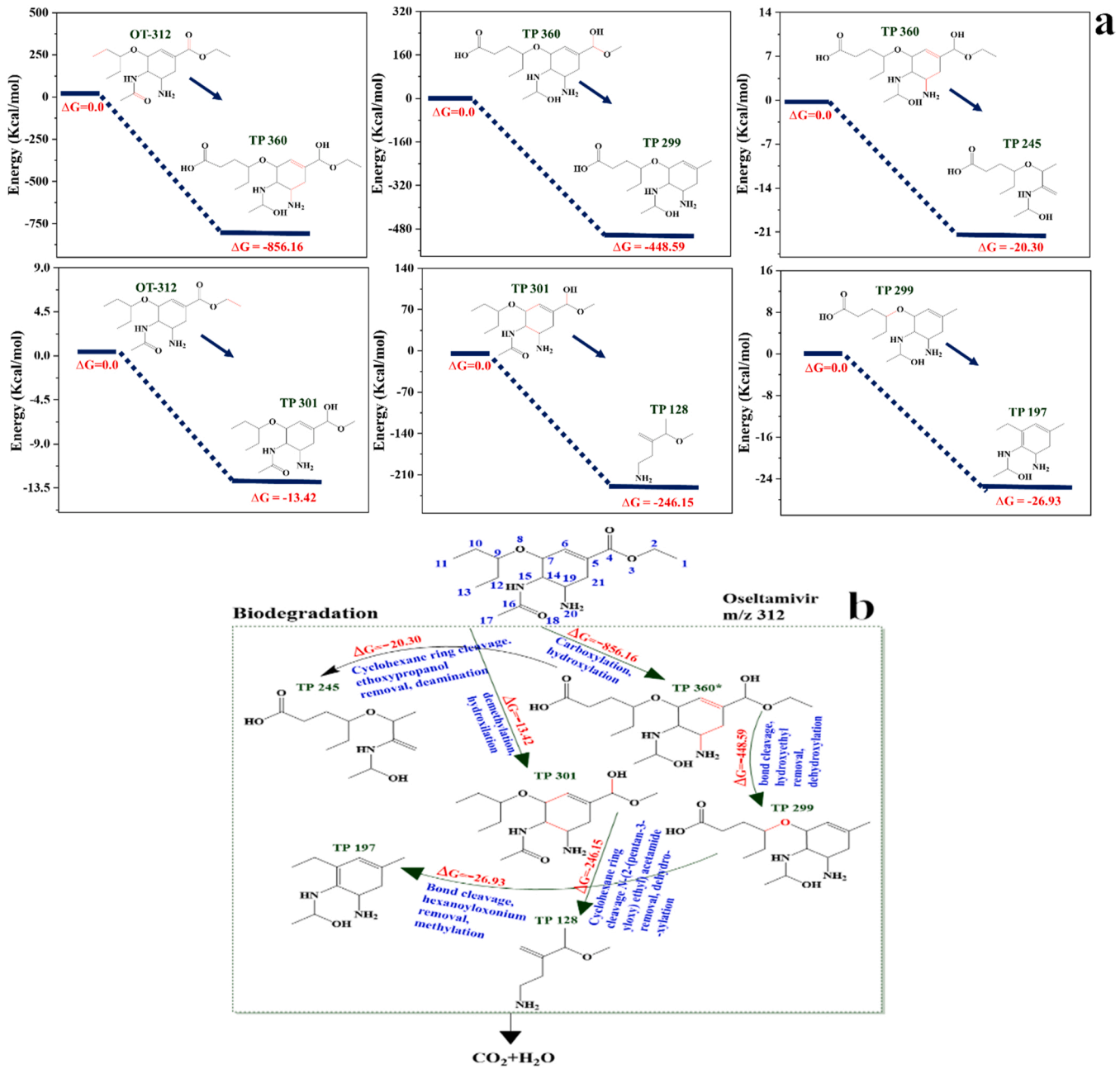

Fig. 6. (a) Gibbs free energy ΔG (Kcal/mol) scheme for transformation products of OT, calculated at 0 K and 1 atm (b) Proposed biodegradation pathways for OT.

ring cleavage with subsequent methylation of algal product TP-299 (ΔG −26.93 Kcal/mol), which was likely attributed to algal methyl-transferases (Xiong et al., 2018). The cyclohexane ring cleavage in TP-301 with substitution of the hydroxyl group by methyl group might generate TP-128 with a strong reaction energy value (ΔG −246.15). Taken together, the aforementioned results suggested that different algal enzyme sets were consistently performing biodegradation, and simpler TPs (e.g., TP-128, TP-197) might be further oxidized and mineralized into CO_2 and H_2O.

3.4. Environmental sustainability assessment of the produced TPs

To inspect the environmental impacts of OT and subsequent TPs, their PBT properties were assessed by the EPI Suite™ and ECOSAR analysis. Table S5 lists the values of five typical physicochemical parameters for OT and its TPs. These include octanol-water partition coefficients (log Kow), air-water partition coefficients (log Kaw), long-range transport (days), bioconcentration factors (BCF), and the chronic value for major environmental food web organisms viz. fish, daphnids, and others (ChV). In compliance with the benchmarking criteria, all the intermediates were characterized with a log Kow of ≤ 5 and, a BCF value of < 5000 L/kg, suggesting that these TPs did not exhibit the risk of bioaccumulation and associated biomagnification (Tepper et al., 2020). Also, according to the PBT criteria proposed by US-EPA and the European Commission (EC), none of the produced TPs exhibited long-range transport potential in water bodies (Table S5). Besides, the ECOSAR analysis indicated that TPs had no potential toxicological impacts due to the ChV values < 10 mg/L (Li et al., 2018), indicating that all identified TPs presented limited toxicity to life resources.

It is thereby reasonable to conclude that all the microalgal-based TPs of OT might prudently meet the practical demands of environmental sustainability. Fig. 7 illustrates a model of the overall OT exposure with EPS as well as the algal cell and the systematic OT metabolic mechanism according to reported-degradation pathways. The execution of mutually collaborative removal mechanisms and the microalgal enzyme-mediated biodegradation revealed the suitability of microalgal remediation as a promising alternative and environmentally friendly technology.

3.5. Environmental significance

This study illustrated microalgal bioremediation as a promising alternative for removing AVDs from wastewater through multiple elimination pathways. With the impressive adaptation and easy nutritional uptake capacities, this technology is considered to be suitable for application in environmental remediation of pharmaceuticals and AVDs in wastewater. Previous reports successfully correlated quantum chemical calculation in chemical reaction systems for studying the radical-mediated degradation pathways of polycyclic aromatic hydrocarbons in soil, water, and atmospheric ecosystems (Gu et al., 2019; Lin et al., 2021; Zhao et al., 2016). To the best of the authors' knowledge, this is the first report that deployed DFT calculations for assessing the microalgal-mediated biodegradation pathways of AVDs in wastewater.

This suggests that the understanding of the biodegradation by microalgal enzyme-mediated reactions also complies with the chemical reaction standards. Thus, it is feasible to apply quantum chemical calculation in studying the microalgal enzyme-catalyzed degradation pathways. Moreover, the appropriate environmental safety profile of microalgal-mediated produced TPs of AVDs in the present work suggests that microalgae treatment technologies could substantially minimize the bioaccumulation and biomagnification of AVDs in food webs. Further

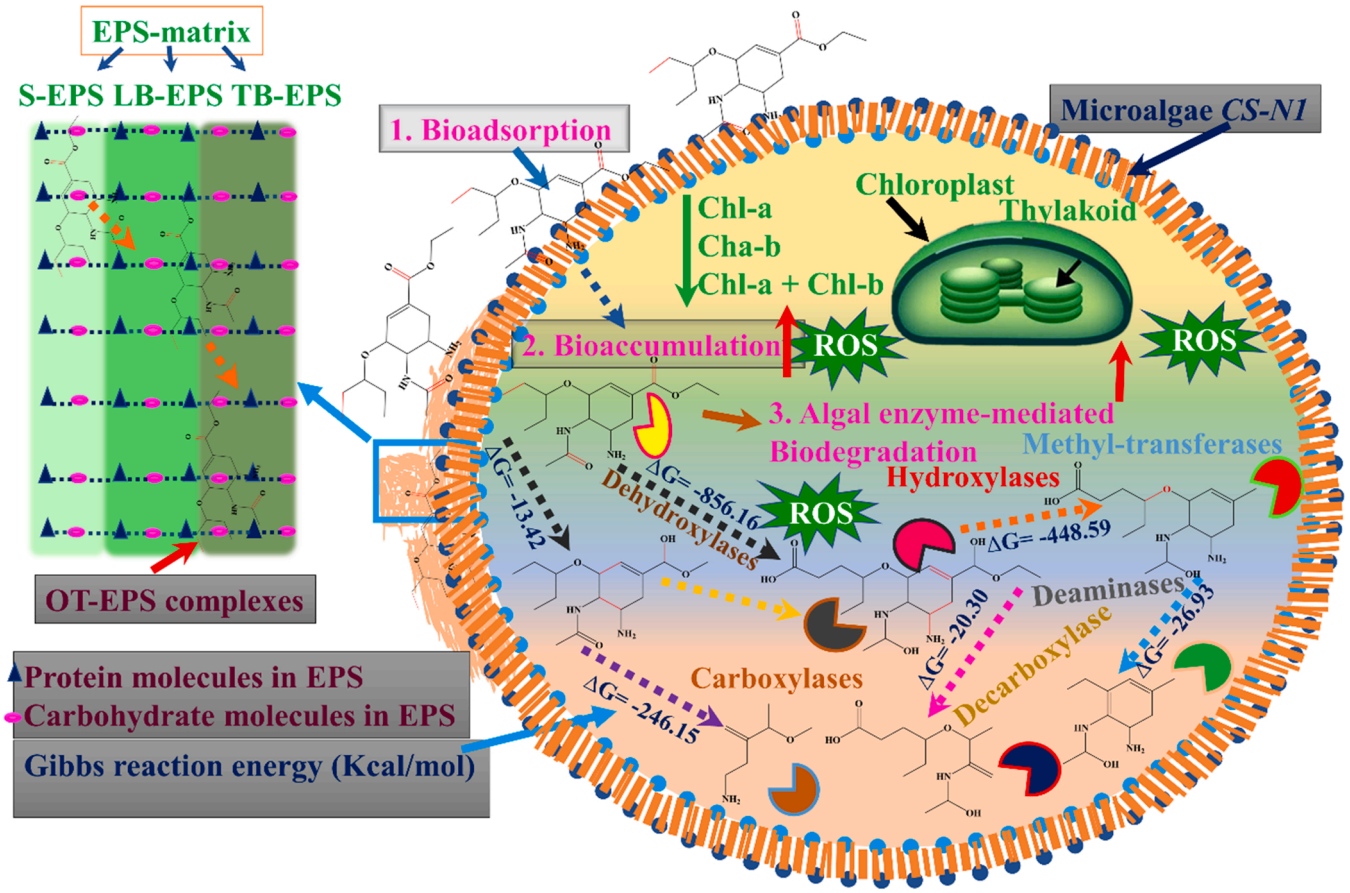

Fig. 7. The proposed illustration of OT interaction with *CS-N1* and it`s systematic metabolic mechanism according to reported enzymatic-degradation pathways.

investigation on the life cycle assessment of the proposed approach will help evaluate its sustainability for remediating the current pharmaceutically-sick ecosystems. Therefore, considering the ecological importance of microalgae in environmentally sustainable remediation principles and increasing AVDs pollution, more studies are recommended to evaluate the adaptive removal strategy of microalgae-based remediation in wastewater treatment.

4. Conclusions

Worldwide wastewater treatment facilities have been challenged by COVID-19-induced AVD consumption. The microalgal system was firstly and successfully exploited against variable dose-treatments of an AVD (OT). This suppression resulted in significant reductions in the microalgal biomass growth, photosynthesis efficiencies, chlorophyll contents, as well as NH_4^+-N and PO_4^{3-}-P uptake. Likewise, complete OT removals were observed in the 10 mg/L OT group while 63% and 54% removal efficiencies were recorded in the 20 mg/L and 30 mg/L groups, respectively. Notably, quantitative and qualitative EPS investigations revealed the EPS secretions correlated well with the cell hydrophobicity in the OT exposed groups. As the primary removal pathway, microalgae-mediated biodegradation was elucidated through experimentation and DFT-supported computation. The environmental sustainability assessment suggested limited toxicity of microalgal-metabolic TPs of OT. Therefore, in the presence of globally elevated AVD consumption and subsequent environmental pollution, systematic and sustainable approaches with microalgae could be a competitive alternative to control of the spread of AVDs in wastewater and recipient environments.

CRediT authorship contribution statement

Qasim M. Zeeshan: Conceptualization, Data curation, Formal Analysis, Investigation, Methodology, Visualization, Writing – original draft, Writing – review & editing. **Shuang Qiu:** Data curation, Formal analysis, Funding Acquisition, Resources, Validation, Writing – review & editing. **Jia Gu:** Data curation, Investigation. **Abdul-Wahab Abbew:** Data curation, Formal Analysis, Methodology, Validation. **Zhengshuai Wu:** Data curation, Investigation. **Zhipeng Chen:** Data curation, Investigation. **Sai Xu:** Conceptualization, Data curation, Investigation, Validation, Visualization. **Shijian Ge:** Conceptualization, Data curation, Formal Analysis, Funding Acquisition, Investigation, Validation, Writing – review & editing, Supervision.

Declaration of Competing Interest

The authors declare that they have no known competing financial interests or personal relationships that could have appeared to influence the reported work in this paper.

Acknowledgments

The authors would like to acknowledge the support of the National Natural Science Foundation of China (52170038 and 52000103), Fundamental Research Funds for the Central Universities (30921011219 and 30920021117), and Natural Science Foundation of Jiangsu Province (BK20190022 and BK20180497). Dr. Shijian Ge acknowledges the support of the Distinguished Professorship of Jiangsu Province and China Association for Science and Technology.

Appendix A. Supporting information

Supplementary data associated with this article can be found in the online version at doi:10.1016/j.jhazmat.2021.128139.

References

Abbew, A.-W., Qiu, S., Amadu, A.A., Qasim, M.Z., Chen, Z., Wu, Z., Wang, L., Ge, S., 2021. Insights into the multi-targeted effects of free nitrous acid on the microalgae Chlorella sorokiniana in wastewater. Bioresour. Technol., 126389
Asharuddin, S.M., Othman, N., Altowayti, W.A.H., Bakar, N.A., Hassan, A., 2021. Recent advancement in starch modification and its application as water treatment agent. Environ. Technol. Innov., 101637
Avila, R., Peris, A., Eljarrat, E., Vicent, T., Blánquez, P., 2021. Biodegradation of hydrophobic pesticides by microalgae: transformation products and impact on algae biochemical methane potential. Sci. Total. Environ. 754, 142114.
Carstensen, A., Herdean, A., Schmidt, S.B., Sharma, A., Spetea, C., Pribil, M., Husted, S., 2018. The impacts of phosphorus deficiency on the photosynthetic electron transport chain. Plant Physiol. 177 (1), 271–284.
Chawla, P., Malik, A., Sreekrishnan, T.R., Dalvi, V., Gola, D., 2020. Selection of optimum combination via comprehensive comparison of multiple algal cultures for treatment of diverse wastewaters. Environ. Technol. Innov. 18, 100758.
Cheah, W.Y., Ling, T.C., Show, P.L., Juan, J.C., Chang, J.-S., Lee, D.-J., 2016. Cultivation in wastewaters for energy: a microalgae platform. Appl. Energy 179, 609–625.
Chen, W.-Y., Wu, Y.-T., Lin, H.-C., Ieong, M.-I., Lee, B.-H., 2020a. Impact of long-term parental exposure to Tamiflu metabolites on the development medaka offspring (Oryzias latipes). Environ. Pollut. 261, 114146.
Chen, Z., Qiu, S., Amadu, A.A., Shen, Y., Wang, L., Wu, Z., Ge, S., 2020b. Simultaneous improvements on nutrient and Mg recoveries of microalgal bioremediation for municipal wastewater and nickel laterite ore wastewater. Bioresour. Technol. 297, 122517.
Chen, Z., Qiu, S., Yu, Z., Li, M., Ge, S., 2021. Enhanced secretions of algal cell-adhesion molecules and metal ion-binding exoproteins promote self-flocculation of Chlorella sp. cultivated in municipal wastewater. Environ. Sci. Technol. 55 (17), 11916–11924.
Chia, S.R., Ong, H.C., Chew, K.W., Show, P.L., Phang, S.-M., Ling, T.C., Nagarajan, D., Lee, D.-J., Chang, J.-S., 2018. Sustainable approaches for algae utilisation in bioenergy production. Renew. Energy 129, 838–852.
Chu, Y., Zhang, C., Ho, S.-H., 2021. Computational simulation associated with biological effects of alkyl organophosphate flame retardants with different carbon chain lengths on Chlorella pyrenoidosa. Chemosphere 263, 127997.
Ding, T., Yang, M., Zhang, J., Yang, B., Lin, K., Li, J., Gan, J., 2017. Toxicity, degradation and metabolic fate of ibuprofen on freshwater diatom Navicula sp. J. Hazard. Mater. 330, 127–134.
Escobar, L., Ballester, P., 2021. Molecular recognition in water using macrocyclic synthetic receptors. Chem. Rev. 121 (4), 2445–2514.
Farhadian, S., Hashemi-Shahraki, F., Asadpour, S., Shareghi, B., Shakerian, B., Rafatifard, M., Firooz, A.R., 2021. Malachite Green, the hazardous materials that can bind to Apo-transferrin and change the iron transfer. Int. J. Biol. Macromol. (2021).
Frisch, M., Trucks, G., Schlegel, H., Scuseria, G., Robb, M., Cheeseman, J., Scalmani, G., Barone, V., Petersson, G., Nakatsuji, H., 2019. Gaussian 16, Revision C. 01, 2016. Gaussian, Inc., Wallingford CT.
Funke, J., Prasse, C., Ternes, T.A., 2016. Identification of transformation products of antiviral drugs formed during biological wastewater treatment and their occurrence in the urban water cycle. Water Res. 98, 75–83.
Gao, Q., Wong, Y., Tam, N.F., 2017. Antioxidant responses of different microalgal species to nonylphenol-induced oxidative stress. J. Appl. Phycol. 29 (3), 1317–1329.
Ge, S., Qiu, S., Tremblay, D., Viner, K., Champagne, P., Jessop, P.G., 2018. Centrate wastewater treatment with Chlorella vulgaris: simultaneous enhancement of nutrient removal, biomass and lipid production. Chem. Eng. J. 342, 310–320.
Gen, M., Zhang, R., Huang, D.D., Li, Y., Chan, C.K., 2019. Heterogeneous SO2 oxidation in sulfate formation by photolysis of particulate nitrate. Environ. Sci. Technol. Lett. 6 (2), 86–91.
Gomaa, M., Zien-Elabdeen, A., Hifney, A.F., Adam, M.S., 2021. Environmental risk analysis of pharmaceuticals on freshwater phytoplankton assemblage: effects on alpha, beta, and taxonomic diversity. Environ. Sci. Pollut. Res. 28 (8), 9954–9964.
Gu, J., Yang, L., Jiang, J., Ma, J., Song, Y., Song, H., Tian, W.Q., 2019. UV photolysis of tetrachloro-p-benzoquinone (TCBQ) in aqueous solution: mechanistic insight from quantum chemical calculations. Chem. Eng. J. 361, 812–819.
Guengerich, F.P., 2018. Mechanisms of cytochrome P450-catalyzed oxidations. ACS Catal. 8 (12), 10964–10976.
Hena, S., Gutierrez, L., Croué, J.-P., 2020. Removal of metronidazole from aqueous media by C. vulgaris. J. Hazard. Mater. 384, 121400.
Hu, J., Li, X., Liu, F., Fu, W., Lin, L., Li, B., 2021. Comparison of chemical and biological degradation of sulfonamides: solving the mystery of sulfonamide transformation. J. Hazard. Mater., 127661
Hu, Y., Meng, F.-L., Hu, Y.-Y., Habibul, N., Sheng, G.-P., 2020. Concentration-and nutrient-dependent cellular responses of microalgae Chlorella pyrenoidosa to perfluorooctanoic acid. Water Res. 185, 116248.
Jia, F., Yang, Q., Liu, X., Li, X., Li, B., Zhang, L., Peng, Y., 2017. Stratification of extracellular polymeric substances (EPS) for aggregated anammox microorganisms. Environ. Sci. Technol. 51 (6), 3260–3268.
Kiki, C., Rashid, A., Wang, Y., Li, Y., Zeng, Q., Yu, C.-P., Sun, Q., 2020. Dissipation of antibiotics by microalgae: kinetics, identification of transformation products and pathways. J. Hazard. Mater. 387, 121985.
Kumar, M., Kuroda, K., Dhangar, K., Mazumder, P., Sonne, C., Rinklebe, Jr, Kitajima, M., 2020. Potential emergence of antiviral-resistant pandemic viruses via environmental drug exposure of animal reservoirs. Environ. Sci. Technol. 54 (14), 8503–8505.
Li, H., Yao, J., Duran, R., Liu, J., Min, N., Chen, Z., Zhu, X., Zhao, C., Ma, B., Pang, W., 2021. Toxic response of the freshwater green algae Chlorella pyrenoidosa to

combined effect of flotation reagent butyl xanthate and nickel. Environ. Pollut. 286, 117285.
Li, J., Su, G., Letcher, R.J., Xu, W., Yang, M., Zhang, Y., 2018. Liquid crystal monomers (LCMs): a new generation of persistent bioaccumulative and toxic (PBT) compounds? Environ. Sci. Technol. 5005–5006.
Lin, J., Dai, Q., Zhao, H., Cao, H., Wang, T., Wang, G., Chen, C., 2021. Photoinduced release of volatile organic compounds from fatty alcohols at the air–water interface: the role of singlet oxygen photosensitized by a carbonyl group. Environ. Sci. Technol. 55 (13), 8683–8690.
Liu, W., Li, Y., Liu, F., Jiang, W., Zhang, D., Liang, J., 2019. Visible-light-driven photocatalytic degradation of diclofenac by carbon quantum dots modified porous g-C3N4: mechanisms, degradation pathway and DFT calculation. Water Res. 151, 8–19.
Lu, X., Xu, W., Liu, C., Zhao, Q., Ye, Z., 2021. Insight into the role of extracellular polymeric substances in denitrifying biofilms under nitrobenzene exposure. Ecotoxicol. Environ. Saf. 222, 112539.
Luo, L., Xiao, Z., Zhou, X., Yang, L., Luo, S., Zhao, C., Luan, T., 2020. Quantum chemical calculation to elucidate the biodegradation pathway of methylphenanthrene by green microalgae. Water Res. 173, 115598.
Mao, Y., Yu, Y., Ma, Z., Li, H., Yu, W., Cao, L., He, Q., 2021. Azithromycin induces dual effects on microalgae: roles of photosynthetic damage and oxidative stress. Ecotoxicol. Environ. Saf. 222, 112496.
Matamoros, V., Uggetti, E., García, J., Bayona, J.M., 2016. Assessment of the mechanisms involved in the removal of emerging contaminants by microalgae from wastewater: a laboratory scale study. J. Hazard. Mater. 301, 197–205.
Mlunguza, N.Y., Ncube, S., Mahlambi, P.N., Chimuka, L., Madikizela, L.M., 2020. Determination of selected antiretroviral drugs in wastewater, surface water and aquatic plants using hollow fibre liquid phase microextraction and liquid chromatography-tandem mass spectrometry. J. Hazard. Mater. 382, 121067.
Mohite, B.V., Koli, S.H., Narkhede, C.P., Patil, S.N., Patil, S.V., 2017. Prospective of microbial exopolysaccharide for heavy metal exclusion. Appl. Biochem. Biotechnol. 183 (2), 582–600.
Nannou, C., Ofrydopoulou, A., Evgenidou, E., Heath, D., Heath, E., Lambropoulou, D., 2020. Antiviral drugs in aquatic environment and wastewater treatment plants: a review on occurrence, fate, removal and ecotoxicity. Sci. Total Environ. 699, 134322.
Naveed, S., Li, C., Zhang, J., Zhang, C., Ge, Y., 2020. Sorption and transformation of arsenic by extracellular polymeric substances extracted from Synechocystis sp. PCC6803. Ecotoxicol. Environ. Saf. 206, 111200.
Olisah, C., Rubidge, G., Human, L.R., Adams, J.B., 2021. A translocation analysis of organophosphate pesticides between surface water, sediments and tissues of common reed Phragmites australis. Chemosphere 284, 131380.
Omar, M.A., Derayea, S.M., Mostafa, I.M., 2017. Selectivity improvement for spectrofluorimetric determination of oseltamivir phosphate in human plasma and in the presence of its degradation product. J. Fluoresc. 27 (4), 1323–1330.
Peter, A.P., Khoo, K.S., Chew, K.W., Ling, T.C., Ho, S.-H., Chang, J.-S., Show, P.L., 2021. Microalgae for biofuels, wastewater treatment and environmental monitoring. Environ. Chem. Lett. 1–14.
Qiu, S., Wang, L., Chen, Z., Yang, M., Yu, Z., Ge, S., 2021a. An integrated mainstream and sidestream strategy for overcoming nitrite oxidizing bacteria adaptation in a continuous plug-flow nutrient removal process. Bioresour. Technol. 319, 124133.
Qiu, S., Yu, Z., Hu, Y., Chen, Z., Guo, J., Xia, W., Ge, S., 2021b. An evolved native microalgal consortium-snow system for the bioremediation of biogas and centrate wastewater: start-up, optimization and stabilization. Water Res., 117038
Qiu, S.W., Chen, Z., Champagne, Z., Abbew, A.-W., Li, P., Ge, S., 2021. Microalgal activity and nutrient uptake from waste water enhanced by nanoscale zerovalent iron: performance and molecular mechanism. Environ. Sci. Technol. https://doi.org/10.1021/acs.est.1c05503.
Rambabu, K., Banat, F., Pham, Q.M., Ho, S.-H., Ren, N.-Q., Show, P.L., 2020. Biological remediation of acid mine drainage: review of past trends and current outlook. Environ. Sci. Ecotechnol. 2, 100024.
Rempel, A., Biolchi, G.N., Antunes, A.C.F., Gutkoski, J.P., Treichel, H., Colla, L.M., 2021. Cultivation of microalgae in media added of emergent pollutants and effect on growth, chemical composition, and use of biomass to enzymatic hydrolysis. Bioenergy Res. 14 (1), 265–277.
Shen, Y., Qiu, S., Chen, Z., Zhang, Y., Trent, J., Ge, S., 2020. Free ammonia is the primary stress factor rather than total ammonium to Chlorella sorokiniana in simulated sludge fermentation liquor. Chem. Eng. J. 397, 125490.
Song, C., Wei, Y., Qiu, Y., Qi, Y., Li, Y., Kitamura, Y., 2019. Biodegradability and mechanism of florfenicol via Chlorella sp. UTEX1602 and L38: experimental study. Bioresour. Technol. 272, 529–534.
Tepper, V., Nykvist, M., Gillman, A., Skog, E., Wille, M., Lindström, H.S., Tang, C., Lindberg, R.H., Lundkvist, Å., Järhult, J.D., 2020. Influenza A/H4N2 mallard infection experiments further indicate zanamivir as less prone to induce environmental resistance development than oseltamivir. J. Gen. Virol. 101 (8), 816–824.
Ubando, A.T., Africa, A.D.M., Maniquiz-Redillas, M.C., Culaba, A.B., Chen, W.-H., Chang, J.-S., 2021. Microalgal biosorption of heavy metals: a comprehensive bibliometric review. J. Hazard. Mater. 402, 123431.
Wang, L., Qiu, S., Guo, J., Ge, S., 2021. Light irradiation enables rapid start-up of nitritation through suppressing nxrb gene expression and stimulating ammonia-oxidizing bacteria. Environ. Sci. Technol. 55 (19), 13297–13305.
Wang, S., Liu, M., Wang, J., Huang, J., Wang, J., 2020a. Polystyrene nanoplastics cause growth inhibition, morphological damage and physiological disturbance in the marine microalga Platymonas helgolandica. Mar. Pollut. Bull. 158, 111403.
Wang, S., Poon, K., Cai, Z., 2018. Removal and metabolism of triclosan by three different microalgal species in aquatic environment. J. Hazard. Mater. 342, 643–650.
Wang, W., Yan, Y., Zhao, Y., Shi, Q., Wang, Y., 2020b. Characterization of stratified EPS and their role in the initial adhesion of anammox consortia. Water Res 169, 115223.
Wang, Z., Lee, Y.-Y., Scherr, D., Senger, R.S., Li, Y., He, Z., 2020c. Mitigating nutrient accumulation with microalgal growth towards enhanced nutrient removal and biomass production in an osmotic photobioreactor. Water Res. 182, 116038.
Wu, D., Li, G.-F., Shi, Z.-J., Zhang, Q., Huang, B.-C., Fan, N.-S., Jin, R.-C., 2019. Co-inhibition of salinity and Ni (II) in the anammox-UASB reactor. Sci. Total Environ. 669, 70–82.
Xie, P., Chen, C., Zhang, C., Su, G., Ren, N., Ho, S.-H., 2020. Revealing the role of adsorption in ciprofloxacin and sulfadiazine elimination routes in microalgae. Water Res. 172, 115475.
Xiong, J.-Q., Kurade, M.B., Jeon, B.-H., 2017. Biodegradation of levofloxacin by an acclimated freshwater microalga, Chlorella vulgaris. Chem. Eng. J. 313, 1251–1257.
Xiong, J.-Q., Kurade, M.B., Jeon, B.-H., 2018. Can microalgae remove pharmaceutical contaminants from water? Trends Biotechnol. 36 (1), 30–44.
Xiong, Q., Liu, Y.-S., Hu, L.-X., Shi, Z.-Q., Cai, W.-W., He, L.-Y., Ying, G.-G., 2020. Co-metabolism of sulfamethoxazole by a freshwater microalga Chlorella pyrenoidosa. Water Res. 175, 115656.
Zhang, C., Chen, X., Chou, W.-C., Ho, S.-H., 2021a. Phytotoxic effect and molecular mechanism induced by nanodiamonds towards aquatic Chlorella pyrenoidosa by integrating regular and transcriptomic analyses. Chemosphere 270, 129473.
Zhang, C., Huang, X., Chu, Y., Ren, N., Ho, S.-H., 2020. An overlooked effect induced by surface modification: different molecular response of Chlorella pyrenoidosa to graphitized and oxidized nanodiamonds. Environ. Sci. Nano 7 (8), 2302–2312.
Zhang, C., Li, S., Ho, S.-H., 2021b. Converting nitrogen and phosphorus wastewater into bioenergy using microalgae-bacteria consortia: a critical review. Bioresour. Technol., 126056
Zhang, G., Wei, S., Wu, B., Chen, Z., Zhang, S., 2018. Nonnegligible generation of hydroxyl radicals from UVC photolysis of aqueous nitrous oxide. Environ. Sci. Technol. 52 (17), 9785–9792.
Zhao, N., Zhang, Q., Wang, W., 2016. Atmospheric oxidation of phenanthrene initiated by OH radicals in the presence of O2 and NOx—a theoretical study. Sci. Total Environ. 563, 1008–1015.
Zou, W., Wan, Z., Zhao, C., Zhang, G., Zhang, X., Zhou, Q., 2021. Impact of algal extracellular polymeric substances on the environmental fate and risk of molybdenum disulfide in aqueous media. Water Res. 205, 117708.